PHYSICAL REVIEW E **92**, 061301(R) (2015)

Entropic lattice Boltzmann model for compressible flows

N. Frapolli,* S. S. Chikatamarla,† and I. V. Karlin‡
Department of Mechanical and Process Engineering, ETH Zurich, 8092 Zurich, Switzerland
(Received 3 July 2015; published 28 December 2015)

We present a lattice Boltzmann model (LBM) that covers the entire range of fluid flows, from low Mach weakly compressible to transonic and supersonic flows. One of the most restrictive limitations of the lattice Boltzmann method, the low Mach number limit, is overcome here by three fundamental changes to the LBM scheme: use of an appropriately chosen multispeed lattice, accurate evaluation of the equilibrium, and the entropic relaxation for the collision. The range of applications is demonstrated through the simulation of a bow shock in front of an airfoil and the simulation of decaying compressible turbulence with shocklets.

DOI: 10.1103/PhysRevE.92.061301 PACS number(s): 47.11.−j, 47.15.−x, 47.40.−x, 51.10.+y

Incompressible and compressible flows are stunningly different [1], with turbulence on one end and shock waves on the other. While the entire range is represented by the fundamental Navier-Stokes (NS) and Fourier equations, the different physics of the two extremes (low and high Mach numbers) has led to the divergent paths that numerical simulations have long followed: higher-order schemes for direct numerical simulation (DNS) of turbulent and weakly compressible flows, and shock-capturing schemes for highly compressible and supersonic cases. The lack of a uniform approach which would bridge these two limits in a natural way is well recognized [2,3]: Compressible flows require high dissipation (for example, near the shock front) to avoid Gibbs oscillations while turbulence requires low dissipative schemes to achieve accurate results. These mutually excluding scenarios caused by the different physics create a fundamental void in the numerical study of flows that involves both the regimes of smooth flow (turbulence) and flows with discontinuities which are an integral part of applications in high-speed aerodynamics, astrophysics, magnetohydrodynamics, etc. Hence, hybrid schemes are a necessity for flows with discontinuities; however, it is believed that the "key role for the success of hybrid methods is played by shock sensors" [2]. Thus, high-fidelity reliable DNSs of compressible or high Mach number flows still remain a challenge for the state-of-the art numerical methods.

More recently, the lattice Boltzmann method (LBM) [4] has emerged as an alternative recast of the Navier-Stokes equations in a form of an overwhelmingly simple kinetic equation for the populations of designer particles $f_i(\boldsymbol{x},t)$, with the simplest rules of propagation on a space-filling lattice formed by discrete velocities $\boldsymbol{v}_i$ in discrete-time steps, and local relaxation at the nodes $\boldsymbol{x}$. At present, LBM has matured into a successful method for incompressible flows [5]. Notably, the entropic lattice Boltzmann method (ELBM) [6–8] has restored the second law of thermodynamics (Boltzmann's H theorem) for the lattice kinetic theory and has enabled high Reynolds number flow simulations. While the success of LB methods has expanded greatly over the past two decades to porous media, multiphase flows, and thermal incompressible flows, all these applications are confined to the low Mach number subdomain of fluid dynamics. The situation is drastically different for compressible flows where numerous attempts to derive a *genuine* lattice Boltzmann model have failed, to date [9–16]. Earlier attempts were heavily reliant on tuning parameters or artificial dissipation arising from inexact propagation, or the introduction of correction terms and similar *ad hoc* techniques. With all this, lattice Boltzmann models for compressible flows drop short of a quantitative comparison to direct numerical simulations, unlike in the case of low Mach numbers.

In this Rapid Communication, we show that the gap between the incompressible and compressible flow computations is covered with an ELBM model that can simulate both turbulence and discontinuous flows. Three fundamental changes to the lattice Boltzmann scheme are introduced here for the development of such a model: the use of a properly chosen multispeed lattice, the accurate entropic equilibrium, and the entropic relaxation for the collision. The capabilities of this model are demonstrated by the simulation of a supersonic bow shock in a flow around an airfoil at a high Reynolds number, and compressible decaying turbulence. An excellent comparison with reference data and the intrinsic simplicity of the fully local ELBM makes it a promising candidate for a direct numerical simulation of compressible flows.

We start by identifying a suitable discrete velocity lattice. The primary guideline is to choose a lattice whose discrete equilibria approximate the moments of the Maxwell-Boltzmann distribution function as close as possible, which in turn ensures the recovery of the NS equations. Using the standard nomenclature $D3Qn$ for the lattices with n speeds in $D=3$ space dimension, the hierarchy of lattices described in Refs. [17,18] is constructed as the tensor products of D copies of one-dimensional velocity sets V_k. The standard $D3Q3^3$ lattice ($V_3=\{0,\pm1\}$) used in incompressible LBM simulations is the lowest member of this hierarchy. We can now derive the lattices $D3Q5^3$ ($V_5=\{0,\pm1,\pm3\}$), $D3Q7^3$ ($V_7=\{0,\pm1,\pm2,\pm3\}$), and so forth. Figure 1 reports the deviation of the equilibrium energy flux $\boldsymbol{q}^{\rm eq}$ from its Maxwell-Boltzmann counterpart $\boldsymbol{q}^{\rm MB}=(\rho/2)\boldsymbol{u}(5T_0+u^2)$ for a few members of the hierarchy as a function of the Mach number $\mathrm{Ma}=u/\sqrt{\gamma_{\rm tr}T_0}$, with $\gamma_{\rm tr}=5/3$ the adiabatic exponent of the ideal gas and T_0 the reference temperature specific to each lattice [17,18] ($k_{\rm B}/m=1$). We note that, moving up the hierarchy of the lattices, the deviation of $\boldsymbol{q}^{\rm eq}$ from $\boldsymbol{q}^{\rm MB}$ drops dramatically. It is also clear from Fig. 1 that the higher-order lattices have

*frapolli@lav.mavt.ethz.ch
†chikatamarla@lav.mavt.ethz.ch
‡Corresponding author: karlin@lav.mavt.ethz.ch

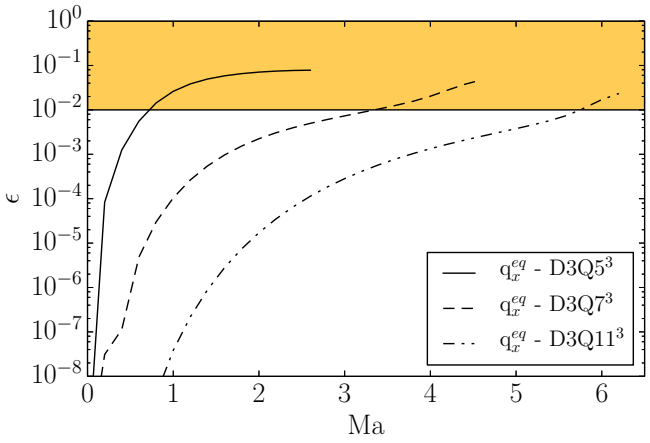

FIG. 1. (Color online) Deviation of the x component of the lattice Boltzmann equilibrium energy flux $q_x^{\rm eq}$ from the Maxwell-Boltzmann value $q_x^{\rm MB}$ as a function of Mach number, $\epsilon = |q_x^{\rm eq} - q_x^{\rm MB}|/|q_x^{\rm MB}|$, is shown for the three members of the lattice hierarchy, $D3Q5^3$, $D3Q7^3$, and $D3Q11^3$. The shaded region indicates a deviation above 1%. Lines are drawn to the limit of existence of the corresponding equilibria.

a robust positivity domain of corresponding equilibria and we can observe that the lattice $D3Q7^3$ is sufficient for the transition from the subsonic to supersonic flow regime. It must be noted that Fig. 1 would not be possible without another key development introduced here, an accurate entropic equilibrium, which is described later.

We now proceed with the construction of the compressible entropic LBM by choosing the entropy function [6]

$$H(f) = \sum_{i=1}^{n} f_i \ln(f_i/W_i), \tag{1}$$

where the weights W_i are determined by seven one-dimensional weights, $w_0 = (36 - 49T + 42T^2 - 15T^3)/36$, $w_{\pm1} = T(12 - 13T + 5T^2)/16$, $w_{\pm2} = T(-3 + 10T - 5T^2)/40$, $w_{\pm3} = T(4 - 15T + 15T^2)/720$, which are in turn derived by matching the first four nonvanishing Maxwell-Boltzmann moments at $u = 0$ [17,18]. The weight W_i of each discrete velocity $\boldsymbol{v}_i$ in the natural Cartesian reference frame, $\boldsymbol{v}_i = (v_{ix}, v_{iy}, v_{iz})$, $i\alpha \in \{0, \pm1, \pm2, \pm3\}$, is the algebraic product of the corresponding one-dimensional weights, $W_i = w_{ix} w_{iy} w_{iz}$. This tensor product of the seven velocity one-dimensional lattice is used for all the two- ($D2Q7^2$) and three-dimensional ($D3Q7^3$) simulations presented here. The local equilibrium is defined as the minimizer of the entropy function (1) subject to the conserved fields of density ρ, momentum $\rho\boldsymbol{u}$, and translational energy $\rho E_{\rm tr} = (3/2)\rho T + \rho u^2/2$,

$$\{\rho, \rho\boldsymbol{u}, \rho E_{\rm tr}\} = \sum_{i=1}^{n} \{1, \boldsymbol{v}_i, v_i^2/2\} f_i^{\rm eq}(\rho, \boldsymbol{u}, T). \tag{2}$$

The key is to evaluate $f_i^{\rm eq}$ accurately. To that end, the minimization problem is solved with the method of the Lagrange multipliers (LMs), leading to

$$\delta H + \delta[\chi\rho + \boldsymbol{\zeta} \cdot (\rho\boldsymbol{u}) + \lambda\rho E_{\rm tr}] = 0, \tag{3}$$

where $\chi(\boldsymbol{u}, T)$, $\boldsymbol{\zeta}(\boldsymbol{u}, T)$, and $\lambda(\boldsymbol{u}, T)$ are Lagrange multipliers corresponding to the conservation of mass, momentum, and translational energy, respectively. The formal solution to the minimization problem reads

$$f_i^{\rm eq} = \rho W_i \exp\left(\chi + \boldsymbol{\zeta} \cdot \boldsymbol{v}_i + \lambda v_i^2\right). \tag{4}$$

This form of the equilibrium contrasts with a conventional derivation [19] that derives the equilibrium from the continuous H function (Maxwell-Boltzmann distribution) and then discretizes it to attain the discrete equilibrium. Such an approach violates the entropy maximum condition (second law) that is valid for the Boltzmann equation. In the case of ELBM, we first discretize the continuous H function and then obtain the equilibrium corresponding to this discrete H function, thus guaranteeing compliance with the second law of thermodynamics.

The function $f_i^{\rm eq}(\rho, \boldsymbol{u}, T)$ needs to be computed by applying the conservation laws (2) on (3) and inverting the 5×5 nonlinear system for Lagrange multipliers in three dimensions (3D). For the evaluation, we apply the rapidly converging Newton-Raphson method to solve for the Lagrange multipliers and obtain the accurate entropic equilibrium at a cost comparable to the regular polynomial form. Our simulations show convergence to an accurate solution [with an error of $O(10^{-8})$] in five iterations on average. It is imperative to remark that the conventional ways of deriving the equilibrium through a Taylor series in the velocity $\boldsymbol{u}$, which was valid in the low Mach number limit, is inapplicable in the present case because the errors accumulate rapidly with increasing Mach number. This explains the failure of earlier attempts to construct a lattice Boltzmann method for compressible flows using a polynomial approximation to the equilibrium [19,20], and is recognized as the major flaw in existing approaches. Moreover, the polynomial form of equilibrium suffers from a limited range of positivity for large deviations from $T = T_0$ and $\boldsymbol{u} = \boldsymbol{0}$ and thus cannot be used in the construction of LB models that are capable of handling large temperature and velocity gradients. Armed with the above method of the accurate evaluation of entropic equilibrium, the ELBM model for compressible flow is written in the standard propagation-relaxation form as

$$f_i(\boldsymbol{x} + \boldsymbol{v}_i, t+1) - f_i(\boldsymbol{x}, t) = \alpha\beta_1\left(f_i^{\rm eq} - f_i\right) + 2(\beta_1 - \beta_2)[f_i^* - f_i^{\rm eq}], \tag{5}$$

where f^* is the quasiequilibrium which controls the Prandtl number [21],

$$f_i^* = f_i^{\rm eq} + W_i \overline{\boldsymbol{Q}} : [\boldsymbol{v}_i \otimes \boldsymbol{v}_i \otimes \boldsymbol{v}_i - 3T\boldsymbol{v}_i \boldsymbol{I}]/(6T^3), \tag{6}$$

where $\overline{\boldsymbol{Q}} = \sum_{i=1}^{n} f_i(\boldsymbol{v}_i - \boldsymbol{u}) \otimes (\boldsymbol{v}_i - \boldsymbol{u}) \otimes (\boldsymbol{v}_i - \boldsymbol{u})$ is the central heat flux tensor, and $\boldsymbol{I}$ is the unit tensor. Finally, the ELBM entropic estimate α in (5) is the third crucial ingredient of the model and is computed as the nontrivial root of the entropy balance,

$$H(f) = H[f + \alpha(f^{\rm eq} - f)]. \tag{7}$$

The entropy estimate (7) is applied in the same way as in the previous realizations of ELBM for turbulence [22], thermal convection [23], and recently also to multiphase flows [24]. We shall comment later on the significance of this key element of ELBM for compressible flows. By a

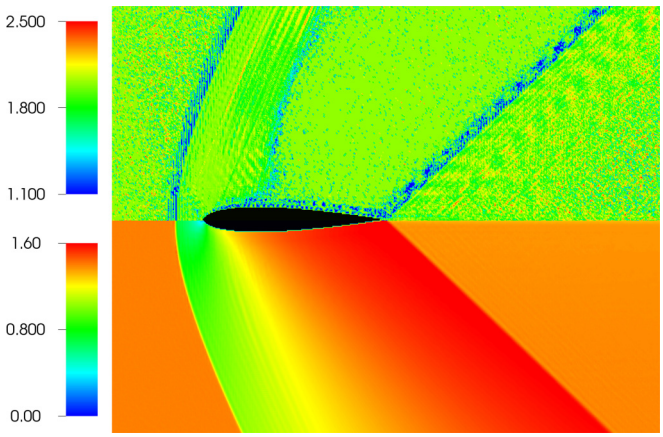

FIG. 2. (Color online) Flow around a NACA0012 airfoil immersed in a supersonic flow field at Ma = 1.4 and Re = 3×10^6 based on chord length and inflow speed. Bottom panel: Mach number distribution. Top panel: Distribution of entropic estimate α. The steady state was reached after 5000 lattice steps.

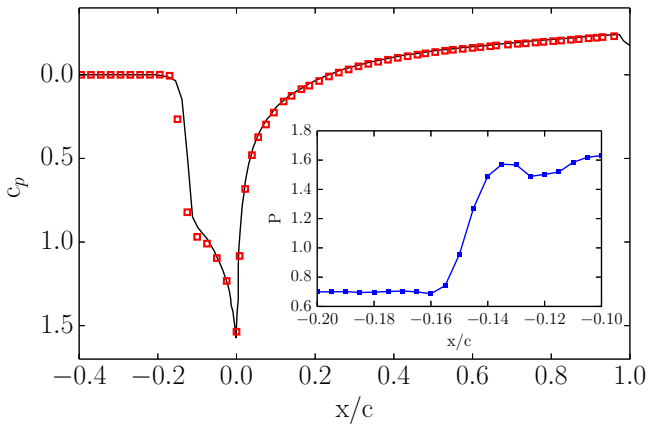

FIG. 3. (Color online) Pressure coefficient c_p upstream and on the NACA0012 airfoil surface. Symbol: ELBM. Line: Supersonic flow solver [26]. Space reduced by chord length c. Inset: Zoom of pressure distribution through the shock.

Chapman-Enskog analysis, we can show that the model (5) recovers equations of compressible hydrodynamics [21], and parameters β_1 and β_2 are related to the kinematic viscosity and thermal diffusivity as $\nu = [1/(2\beta_1) - 1/2]T$ and $\kappa = C_p[1/(2\beta_2) - 1/2]T$, respectively; the Prandtl number is thus $\mathrm{Pr} = (1-\beta_1)\beta_2/(1-\beta_2)\beta_1$. The model (5) is restricted to a fixed value of adiabatic exponent $\gamma_{\mathrm{tr}} = 5/3$ owing to the fact that f_i^{eq} was matched to the Maxwell-Boltzmann distribution for a monatomic gas. This restriction is removed following the idea of Rykov's kinetic model for diatomic molecules [25] and introducing another set of populations g_i which carry the energy related to internal degrees of freedom (rotational and vibrational) and thus enabling a variable γ. The kinetic equation for g populations is written as

$$g_i(\boldsymbol{x}+\boldsymbol{v}_i,t+1) - g_i(\boldsymbol{x},t) = \alpha\beta_1\left(g_i^{\mathrm{eq}} - g_i\right) + 2(\beta_1-\beta_2)[g_i^{*} - g_i^{\mathrm{eq}}]. \quad (8)$$

Equilibrium g_i^{eq} accounts for the conservation of the energy stored in the internal degrees of freedom $E_{\mathrm{int}} = \sum_{i=1}^{n} g_i^{\mathrm{eq}} = (C_{\mathrm{v}} - 3/2)\rho T$, where C_{v} is the specific heat at constant volume. The conservation law for the total energy is now written as

$$\rho E_{\mathrm{tot}} = C_{\mathrm{v}}\rho T + \rho(u^2/2) = \sum_{i=1}^{n}(v_i^2/2) f_i^{\mathrm{eq}} + \sum_{i=1}^{n} g_i^{\mathrm{eq}}, \quad (9)$$

and the adiabatic exponent is now related to a variable specific heat at constant volume C_{v} by $\gamma = (C_{\mathrm{v}}+1)/C_{\mathrm{v}}$. Note that the equilibrium g_i^{eq} does not need to be computed by another Newton-Raphson iteration; once f_i^{eq} is evaluated, we set $g_i^{\mathrm{eq}} = (C_{\mathrm{v}} - 3/2)T f_i^{\mathrm{eq}}$. The quasiequilibrium g_i^{*} is defined consistently to f_i^{*} as $g_i^{*} = g_i^{\mathrm{eq}} + W_i \overline{\boldsymbol{q}} \cdot \boldsymbol{v}_i / T$, where $\overline{\boldsymbol{q}} = \sum_{i=1}^{n} g_i(\boldsymbol{v}_i - \boldsymbol{u})$ is the contracted centered heat flux tensor associated with the internal degrees of freedom. With this formulation, Eqs. (5) and (8), the Reynolds number, the Prandtl number, and the adiabatic exponent γ can be set independently. Below, we consider air with $\mathrm{Pr} = 0.7$ and $\gamma = 1.4$.

This ELB model for thermal and compressible flows is validated in both two and three dimensions for subsonic, transonic, and supersonic regimes. First, we consider a two-dimensional flow around an airfoil immersed in a supersonic flow at Mach number Ma = 1.4 and Reynolds number Re = 3×10^6 and a grid resolution of $c = 200$ for the chord of the airfoil. To compare our simulation results to the solution of Euler equations, free slip boundary conditions on the airfoil surface were implemented according to Ref. [21]. Inlet boundary conditions are applied by enforcing equilibrium at target inlet quantities. An outlet boundary condition is implemented by restoring previous time-step populations at the outlet nodes. The top and bottom boundaries are set to guarantee periodicity. The expected stationary bow shock is clearly visible in the Mach distribution presented in Fig. 2. For this setup, we compare the pressure coefficient $c_p = (P - P_\infty)/(0.5\rho u_\infty^2)$ upstream and on the airfoil surface to the specialized Euler solver [26] in Fig. 3. The ELBM result is in excellent agreement with the supersonic flow solver, which is considered to be the state of the art for such flow setups.

The significance of the entropic estimate is demonstrated in Fig. 2 by showing the distribution of α (7). Note that α deviates significantly from the near-equilibrium value $\alpha = 2$ [6] in the regions near the shock waves, thus damping the Gibbs oscillations. This is demonstrated by the inset in Fig. 3 with a zoom into the inner structure of the bow shock: Only small amplitude oscillations appear and they are confined in the near-shock region. Also, the shock front is resolved with just five to seven grid points. This provides evidence that the fully explicit and purely local ELBM, free of any tuning parameter, is able to stabilize the shock automatically and on demand.

To further validate the capability of ELBM as a predictive method for subsonic and supersonic turbulent flows, we consider here a 3D simulation of compressible decaying turbulence following the direct numerical simulations of Ref. [27]. Two cases were considered. Case 1 is representative of the subsonic regime, with a starting Taylor microscale Reynolds number $\mathrm{Re}_\lambda = 72$ and turbulent Mach number $\mathrm{Ma}_t = 0.1$; case 2 covers the transonic and supersonic regimes with $\mathrm{Re}_\lambda = 175$ and $\mathrm{Ma}_t = 0.488$. Simulations were performed on a uniform cubic grid of $L = 320$ points and the initial turbulent velocity field was generated by random Fourier modes according to

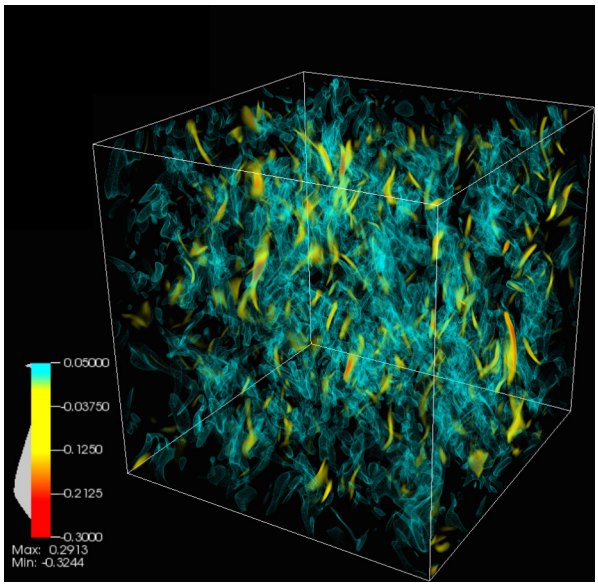

FIG. 4. (Color online) Volume rendering of velocity divergence $\nabla \cdot \boldsymbol{u} < 0$ for decaying compressible turbulence simulation at $t/\tau = 1.56$ (eddy turnover time $\tau = 107.04$ in lattice units) for case 2. High compression domains (shocklets) are seen here in red.

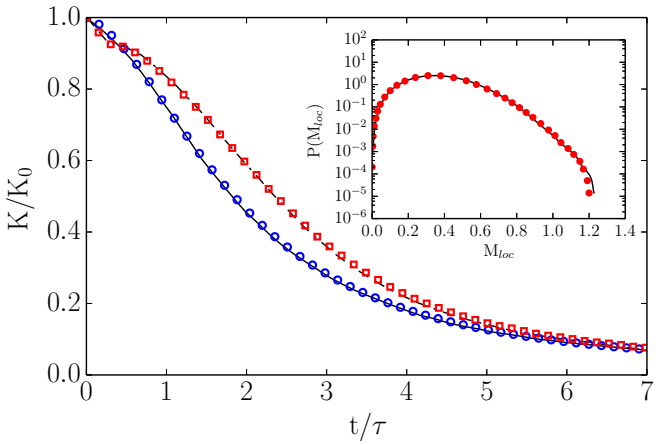

FIG. 5. (Color online) Reduced turbulent kinetic energy K/K_0 vs reduced time t/τ for the lower ($\tau = 223.36$) and higher ($\tau = 85.62$) turbulent Mach number. Case 1: DNS [27] (solid line) and ELBM (circles). Case 2: DNS [27] (dashed line) and ELBM (squares). Inset: pdf of local Mach number at $t/\tau = 1.56$ for Case 2. Line: DNS [27]. Symbol: ELBM.

the energy spectrum of the form $E(k) = Ak^4 \exp(-2k^2/k_0^2)$, and uniform pressure and density similar to Ref. [27]. In case 1, the local Mach number $\mathrm{Ma_{loc}}$ never exceeds the sonic threshold. However, in case 2, $\mathrm{Ma_{loc}}$ can reach values around $\mathrm{Ma_{loc}} = 1.5$. Figure 4 shows the appearance of shocklets (high negative values of flow divergence $\nabla \cdot \boldsymbol{u}$) which were also reported in Ref. [27]. Figure 5 shows excellent agreement for the decay of turbulent kinetic energy for cases 1 and 2, along with the probability distribution function (pdf) of the local Mach number for case 2.

Summarizing, it is remarkable to note that the entropic lattice Boltzmann method and its formulation remain the same for isothermal, multiphase, multicomponent, and here finally for compressible flow simulations. The above ELBM is a physical model which recasts the compressible flow problem into a fully local and intrinsically simple computational framework of the true lattice Boltzmann schemes. With one single algorithm presented above, it is now possible to simulate a broad range of applications ranging from low Mach number flows to transonic and supersonic flow regimes also in the presence of arbitrarily complex obstacles. This is in sharp contrast to NS solvers which require identification of different flow regimes and employing the appropriate numerical approach for it. This breakthrough was possible only by the accurate evaluation of entropic equilibrium and entropic relaxation on an appropriate lattice. In contrast to state-of-the-art fluid solvers, all ELBM simulations are performed using Cartesian meshes without any grid refinement, turbulence model, tuning parameters, or tracking of the shock front. This, when viewed in combination with the simplicity of the LB methods, could make ELBM a competitive and viable option for compressible flow simulations.

This work was supported by the ERC Advanced Grant No. 291094-ELBM. Computational resources at the Swiss National Super Computing Center CSCS were provided under Grant No. s492. Useful discussions with F. Bösch and B. Dorschner are gratefully acknowledged.

[1] L. D. Landau and E. M. Lifshitz, *Fluid Mechanics* (Butterworth-Heinemann, Oxford, U.K., 1987).
[2] S. Pirozzoli, Annu. Rev. Fluid Mech. **43**, 163 (2011).
[3] J. A. Ekaterinaris, Progr. Aerospace Sci. **41**, 192 (2005).
[4] S. Succi, *The Lattice-Boltzmann Equation for Fluid Dynamics and Beyond* (Oxford University Press, Oxford, U.K., 2001).
[5] S. Succi, Europhys. Lett. **109**, 50001 (2015).
[6] I. V. Karlin, A. Ferrante, and H. C. Öttinger, Europhys. Lett. **47**, 182 (1999).
[7] B. M. Boghosian, J. Yepez, P. V. Coveney, and A. Wagner, Proc. R. Soc. London, Ser. A **457**, 717 (2001).
[8] S. Ansumali, I. V. Karlin, and H. C. Öttinger, Europhys. Lett. **63**, 798 (2003).
[9] F. J. Alexander, S. Chen, and J. D. Sterling, Phys. Rev. E **47**, R2249(R) (1993).
[10] Y. Chen, H. Ohashi, and M. Akiyama, Phys. Rev. E **50**, 2776 (1994).
[11] G. McNamara, A. Garcia, and B. Alder, J. Stat. Phys. **81**, 395 (1995).
[12] X. He, S. Chen, and G. D. Doolen, J. Comput. Phys. **146**, 282 (1998).
[13] C. Sun and A. T. Hsu, Phys. Rev. E **68**, 016303 (2003).
[14] T. Kataoka and M. Tsutahara, Phys. Rev. E **69**, 035701(R) (2004).
[15] Z. Guo, C. Zheng, B. Shi, and T. S. Zhao, Phys. Rev. E **75**, 036704 (2007).

[16] Y. Wang, Y. L. He, Q. Li, G. H. Tang, and W. Q. Tao, Int. J. Mod. Phys. C **21**, 383 (2010).
[17] S. S. Chikatamarla and I. V. Karlin, Phys. Rev. Lett. **97**, 190601 (2006).
[18] I. Karlin and P. Asinari, Physica A **389**, 1530 (2010).
[19] X. Shan and X. He, Phys. Rev. Lett. **80**, 65 (1998).
[20] P. C. Philippi, L. A. Hegele, Jr., L. O. E. dos Santos, and R. Surmas, Phys. Rev. E **73**, 056702 (2006).
[21] N. Frapolli, S. S. Chikatamarla, and I. V. Karlin, Phys. Rev. E **90**, 043306 (2014).
[22] S. S. Chikatamarla, C. E. Frouzakis, I. V. Karlin, A. G. Tomboulides, and K. B. Boulouchos, J. Fluid Mech. **656**, 298 (2010).
[23] I. V. Karlin, D. Sichau, and S. S. Chikatamarla, Phys. Rev. E **88**, 063310 (2013).
[24] A. Mazloomi M, S. S. Chikatamarla, and I. V. Karlin, Phys. Rev. Lett. **114**, 174502 (2015).
[25] V. Rykov, Fluid Dyn. **10**, 959 (1975).
[26] M. Hafez and E. Wahba, Int. J. Numer. Methods Fluids **47**, 491 (2005).
[27] R. Samtaney, D. I. Pullin, and B. Kosovic, Phys. Fluids **13**, 1415 (2001).